

Highly Conductive, Scalable, and Machine Washable Graphene-Based E-Textiles for Multifunctional Wearable Electronic Applications

Shaila Afroj, Sirui Tan, Amr M. Abdelkader, Kostya S. Novoselov,* and Nazmul Karim*

Graphene-based textiles show promise for next-generation wearable electronic applications due to their advantages over metal-based technologies. However, current reduced graphene oxide (rGO)-based electronic textiles (e-textiles) suffer from poor electrical conductivity and higher power consumption. Here, highly conductive, ultraflexible, and machine washable graphene-based wearable e-textiles are reported. A simple and scalable pad-dry-cure method with subsequent roller compression and a fine encapsulation of graphene flakes is used. The graphene-based wearable e-textiles thus produced provide lowest sheet resistance ($\approx 11.9 \Omega \text{ sq}^{-1}$) ever reported on graphene e-textiles, and highly conductive even after 10 home laundry washing cycles. Moreover, it exhibits extremely high flexibility, bendability, and compressibility as it shows repeatable response in both forward and backward directions before and after home laundry washing cycles. The scalability and multifunctional applications of such highly conductive graphene-based wearable e-textiles are demonstrated as ultraflexible supercapacitor and skin-mounted strain sensors.

1. Introduction

Wearable electronic devices and systems have become a recent area of interest, where electronic textiles (e-textiles) have emerged as a new generation of wearable devices. The integration of electronic devices such as energy storage systems,^[1,2] health monitoring devices,^[3-7] wearable displays,^[8] and activity monitoring^[9,10] with everyday clothing has changed the paradigm of the next generation textiles. Wearable e-textiles technology that currently exist in the market generally uses complex and time-consuming specialized sewing, knitting, weaving, embroidery, or braiding techniques with conductive yarns or threads.^[11,12] Therefore, the current key trend of wearable e-textiles is to move toward full integration of devices through coating or printing that offers more flexibility, stretchability, and comfort to users.^[13]

Moreover, existing metal-based technologies are expensive,^[14] often toxic and nonbiodegradable.^[15] Furthermore, the higher processing temperature of metallic inks may limit the choice of textile materials which can be used. Therefore, it is essential to develop an alternative to metal-based technologies for wearable e-textiles applications.

Graphene-based wearable e-textiles have attracted significant interest in recent years due to graphene's extraordinary properties such as excellent electrical, mechanical, and other properties.^[16-20] In our previous works,^[21,22] we demonstrated that reduced graphene oxide (rGO), a form of graphene, shows better adhesion to textiles due to the interaction between functional groups of textiles and residual oxygen-containing functional groups of rGO possibly via covalent and hydrogen bonding. Therefore, rGO-based textiles show better washing stability, which is one of the key requirements for wearable e-textiles. However, rGO suffers from poor electrical conductivity due to the defects in the crystal structure and partial restoration of the sp^2 structure of graphene during the reduction process.^[23] Therefore, it may not be suitable for some applications where very high electrical conductivity is required. For such applications graphene-based highly conductive ink could be a possible solution; however there exists two main challenges with such graphene-based inks for wearable e-textiles applications: a) scalable production of highly conductive graphene-based inks and b) the interaction of textiles with


Dr. S. Afroj, Prof K. S. Novoselov, Dr. N. Karim
National Graphene Institute (NGI)
The University of Manchester
Booth Street East, Manchester M13 9PL, UK
E-mail: kostya@manchester.ac.uk; nazmul.karim@uwe.ac.uk

S. Tan
Department of Materials
The University of Manchester
Oxford Road, Manchester M13 9PL, UK

Dr. A. M. Abdelkader
Department of Design and Engineering
Bournemouth University
Dorset BH12 5BB, UK

Prof K. S. Novoselov
Chongqing 2D Materials Institute
Liangjiang New Area, Chongqing 400714, China

Dr. N. Karim
Centre for Fine Print Research
University of West of England
Bristol BS3 2JT, UK

 The ORCID identification number(s) for the author(s) of this article can be found under <https://doi.org/10.1002/adfm.202000293>.

© 2020 The Authors. Published by WILEY-VCH Verlag GmbH & Co. KGaA, Weinheim. This is an open access article under the terms of the Creative Commons Attribution License, which permits use, distribution and reproduction in any medium, provided the original work is properly cited.

DOI: 10.1002/adfm.202000293

chemically inert graphene or graphitic inks. Therefore, there remains a need to produce highly conductive and washable wearable e-textiles in a scalable quantity.

The manufacturing of highly conductive glass rovings was reported using graphene-based inks, which were produced via microfluidization technique.^[24] Microfluidization is a very well-established technique for applications such as de-agglomerating and dispersing carbon nanotubes^[25] and oil-in-water nanoemulsions.^[26] Such method applies a high pressure (up to 207 MPa)^[25] to the entire volume of liquid to pass through a microchannel (diameter, $d < 100 \mu\text{m}$). Therefore, the benefit of this technique over other liquid-phase exfoliations of graphene (shear mixing and ultrasonication) is that it acts over the full volume of the liquid, thus achieves better yield.^[27] It is possible to develop highly concentrated graphene-based conductive inks using such technique, that can be used to produce highly conductive textile fibers. However, such graphene-based textiles suffer from poor washing stability due to the absence of oxygen-containing functional groups in their structure unlike rGO-based textiles. Therefore, there remains a need for the technology that would provide much better washing stability and durability of such conductive textiles. Previous studies^[11,28] reported encapsulation of electrically conductive printed track onto textiles, however based on printed metal inks on textiles which are expensive,^[29] nonbiodegradable,^[15] and not friendly.^[30]

Here, a potential solution for highly conductive wearable e-textiles is reported. Highly scalable microfluidization technique was used to exfoliate concentrated graphene dispersions in water. Then a simple and readily scalable pad-dry-cure (padding) method was used to coat poly-cotton textiles with graphene-based dispersion, that could potentially produce 150 m conductive e-textiles in just 1 min. The electrical conductivity of produced graphene-based e-textile was further improved by a fast compression rolling process, which provides the lowest sheet resistance ($\approx 11.92 \Omega \text{ sq}^{-1}$) ever reported on any graphene-based e-textiles Table S1, Supporting Information. The coated and compressed textile was then encapsulated via screen printing of a thin protecting encapsulant layer before washing 10 times in a home laundry machine. The potential applications of as prepared highly conductive and machine washable graphene-based textiles are also demonstrated as ultraflexible supercapacitor and skin-mounted strain sensor.

2. Results and Discussion

2.1. Highly Conductive Graphene-Based E-Textiles

Few layer graphene was exfoliated using a simple and environmentally friendly microfluidization technique.^[24,27] The statistical analysis of flake thickness, measured by atomic force microscopy (AFM), shows that 20% of exfoliated G flakes are $< 10 \text{ nm}$ thick (Figure S1a, Supporting Information) and the lateral size of the G flakes reduces from ≈ 50 to $\approx 1.5 \mu\text{m}$ after 20 cycles (Figure S1b, Supporting Information). Typical Raman spectra of G flakes show the characteristic features of multi-layers graphene, i.e., G peak at $\approx 1582 \text{ cm}^{-1}$ and an asymmetric 2D band at $\approx 2700 \text{ cm}^{-1}$ ^[31] (Figure S1c, Supporting Information), confirming the successful exfoliation. The broad peak at

$\approx 1350 \text{ cm}^{-1}$, D band, is a sign of some defects introduced into graphene during the exfoliation.^[32,33] However, the I_D/I_G ratio still way lower than that reported for G flakes produced by other liquid phase exfoliation methods.^[33] XPS analysis of exfoliated G flakes reveals that the C/O ratio is much higher (≈ 24.84) than of that of typical rGO ($\approx 10-16$),^[34-36] GO (1-3)^[34] and even in some cases CVD grown pristine graphene (≈ 20).^[37] The high resolution C1s spectrum of G flakes is dominated by a C-C/C=C bond, similar to graphite. The absence of any oxide group peaks confirming the high purity of the produced graphene (Figure S1d,e, Supporting Information). TGA analysis shows slight decomposition ($\approx 2 \text{ wt}\%$) of starting graphite at around $750 \text{ }^\circ\text{C}$, whereas a higher quantity of exfoliated G flakes ($\approx 5.5 \text{ wt}\%$) decomposes at around the same temperature, possibly due to the lower thermal stability of smaller graphene flakes (Figure S1f, Supporting Information).^[38]

A highly scalable pad-dry-cure fabrication technique that could potentially produce graphene-based textiles at very high speed ($\approx 150 \text{ m min}^{-1}$) was used.^[21] The number of coating (padding) cycles was optimized. After the first padding cycle, the sheet resistance of the coated fabric is found to be $\approx 32.7 \text{ k}\Omega \text{ sq}^{-1}$ (Figure 1a). The sheet resistance reduces significantly to $\approx 422 \Omega \text{ sq}^{-1}$ after the second padding cycle and continues to decrease steadily upto 5 padding cycles, due to the deposition of an increased quantity of G flakes on the fabric surface.^[21] Also, the higher number of padding cycles is expected to improve the connectivity between the G flakes due to the applied compression forces from the padding rollers. As it reaches the saturation point, the sheet resistance decreases slowly afterwards. Five padding cycles were used to prepare graphene-coated samples for subsequent processes. It is worth mentioning here that all the samples were dried at $100 \text{ }^\circ\text{C}$ for 5 min after each padding cycle. The curing temperature and time were then optimized for graphene-coated samples. Figure 1b shows that the sheet resistance of G-coated fabric decreases with the increase of curing temperature and time, as it facilitates the evaporation of residual solvents,^[39] hence removes any functional groups that may present on graphene sheet's surface and create some barrier between the individual flakes.^[40] However, the sheet resistance starts to increase after $\approx 150 \text{ }^\circ\text{C}$, possibly due to the degradation of fiber structures, the intramacromolecular cross-linking and depolymerization.^[41,42]

Kawabata evaluation system for fabrics (KES-F) was used to evaluate hand qualities (e.g., softness or stiffness and smoothness) of graphene-coated fabric as perceived by human touch.^[43] Like rGO-coated fabrics in our previous study,^[21] the hand properties of the graphene-coated fabric is not deteriorated after coating with G flakes (Figure 1c). The wide scan XPS spectra of control and optimized graphene-coated poly-cotton fabric show that C/O increases from ≈ 2.83 to ≈ 18.16 after coating with G flakes (Figure S2a, Supporting Information). This is due to the covering of the oxygen functional groups on the cotton fabric with the G flakes, which is also evident from the scanning electron microscope (SEM) images (Figure S3a-c, Supporting Information). The high-resolution C1s spectrum further confirmed the successful and homogeneous coating of the fabric by G flakes. The C1s spectrum of the control poly-cotton reveals that three main peaks can be fitted into three components

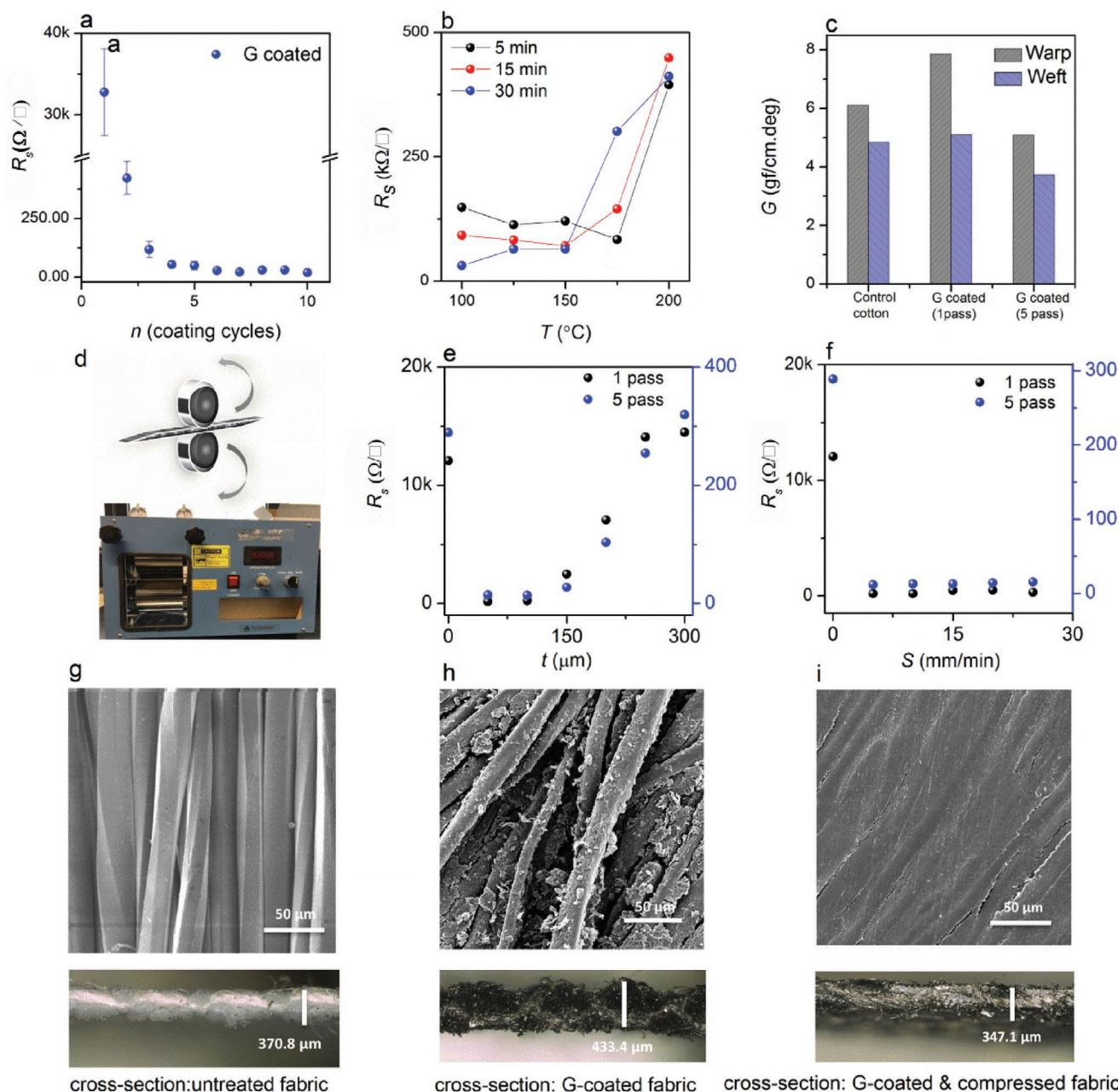


Figure 1. a) The change in the sheet resistance with the number of coating cycle for G-coated poly-cotton fabric. b) The change in sheet resistance of G-coated poly-cotton fabric with curing time and temperature. c) The shear rigidity, G of control poly-cotton and G-coated (1 and 5 passes) poly-cotton fabric in warp and weft direction. d) Schematic diagram of two rotating compression rollers (top) and compression roller instrument (bottom). e) The change in the sheet resistance of G-coated poly-cotton fabric with the change in gap between two compression rollers. f) The change in the sheet resistance of G-coated poly-cotton fabric with the change in speed of compression rollers. g) Scanning electron microscope (SEM) image of control poly-cotton fabric (top) and the average thickness of control poly-cotton fabric in x-section view (bottom). h) SEM image of G-coated (5 passes) poly-cotton fabric and the average thickness of G-coated (5 passes) poly-cotton fabric in x-section view. i) SEM image of G-coated (5 passes) and compressed (with 10 mm gap between compression rollers and 10 mm min⁻¹ speed) poly-cotton fabric (top) and the average thickness of G-coated (5 pass) poly-cotton fabric after compression (with 10 mm gap between compression rollers and 10 mm min⁻¹ speed) in x-section view.

arising from the C–C bond (≈ 284.6 eV), C–O groups (hydroxyl, ≈ 286.2 eV), and C=O/O–C–O groups (carbonyl and acetyl, ≈ 288 eV) (Figure S2b, Supporting Information). However, after coating with G flakes, the signal from the oxygen-containing groups decreased significantly, and the C1s spectrum is dominated by the C–C bond (Figure S2c, Supporting Information).

The higher electrical conductivity is one of the key requirements for wearable e-textiles application.^[44] Most of the graphene e-textiles reported so far are based on rGO,^[21,22] and they suffer from poor electrical conductivity. Although single layer graphene shows incredible electrical properties at an atomic level, the challenge is to retain those properties when

assembled and applied on a substrate in bulk quantities. Previous studies^[45–47] suggested that the use of a suitable post-treatment can improve the electrical conductivity of graphene-based paper substrates such as roller-compression or photonic annealing with subsequent compression rolling. The aim of such posttreatments is generally to decrease the intersheet distance of graphene flakes. In a previous study, the electrical conductivity is increased by nearly an order of magnitude by reducing the average intersheet distance from 3.86 to 3.70 Å.^[40] Moreover, the combination of thermal annealing and subsequent compression rolling reduces the thickness of graphene-printed polyamide and improves electrical conductivity significantly.^[48]

Here, a roller compression method was used to reduce the intersheet distance and consequently improve the electrical conductivity of graphene-based e-textiles (Figure 1d). G-coated textiles were passed through two compression rollers (Figure 1d, top). The gap between the two rollers (t) and the speed of the rollers (S) were optimized. As seen in Figure 1e, the sheet resistance of compressed graphene-coated fabrics increases with the increase of t for both 1 and 5 padding cycles. Similarly, the sheet resistance of compressed graphene-based fabrics increases slightly with the increase of the speed of the rollers (S) (Figure 1f). The average thickness of control, G-coated (5 passes) and compressed poly-cotton fabrics is found to be ≈ 370.8 , ≈ 433.4 , and ≈ 347.1 μm , respectively (Figure 1g–i). Although $t = 300$ μm is lower than the average thickness of G-coated (5 passes) fabrics, the sheet resistance is increased after compression at 300 μm gap between the roller, possibly due to the delamination or removal of unfixed G flakes from the surface. The sheet resistance then decreases with the increase of t , as the intersheet distance between G flakes is reduced.^[45] At $t = 100$ μm , the sheet resistance of G-coated fabric is reduced significantly to ≈ 228.41 Ω sq^{-1} (1 padding cycle) and ≈ 11.92 Ω sq^{-1} (5 padding cycles) by compression. When $t < 100$ μm , a minimal reduction in sheet resistance is observed after compression. However, the compressed fabric become fragile and brittle at $t < 100$ μm and can be torn with very little force, possibly due to the damage of the fabric structure at higher roller pressure. Therefore $t = 100$ μm was used as an optimized gap between the rollers for subsequent processing.

Figure 1g (top) shows a smooth and featureless surface of poly-cotton fiber. However, the fabric is rough and porous with protruding fibers coming out of the surface as evident from the cross-sectional image, Figure 1g (bottom). After coating with G flakes, Figure 1h (top) shows the deposition of a large quantity of G flakes on the fiber surface and a significant increase in the average thickness, Figure 1h (bottom). However, Figure 1i (bottom) shows that the thickness of the G-coated fabric decreases significantly after the compression with two rotating rollers even lower than the control fabric, as the surface become smoother and uniform, Figure 1i (top). The two rotating rollers compress graphene flakes with a high pressure to form a compact film with excellent electrical, mechanical, and thermal properties.^[45,46] Moreover, G flakes are almost indistinguishable on the fiber surface as compression provides strong adhesion between flakes and with the substrate possibly via forming strong attractive van der Waals bonds.^[48]

2.2. Machine Washable Graphene-Based E-Textiles

The washing stability of G-coated textiles was performed to evaluate their performance upto 10 home laundry washing cycles by following a British Standard (BS EN ISO 105 C06 A1S). As found in previous work,^[21,22] rGO demonstrates better adherence with the textile fiber, where residual oxygen-containing functional groups of rGO create hydrogen bondings with that of the textile fibers, thus exhibiting improved wash fastness. Although G-coated e-textiles show excellent electrical conductivity, they demonstrate poor wash stability due to the absence of such oxygen functional groups in G flakes (Figure S1d,e, Supporting Information). The graphene-coated poly-cotton fabric (with 5 padding passes) starts losing electrical conductivity just after one washing cycle. The washing stability improves slightly after roller compression, however G-coated and compressed fabric loses the electrical conductivity drastically after repeated washing cycles, as the sheet resistance increases by 6 orders of magnitudes after 10 washing cycles (Figure 2a). Moreover, a significant variation in the resistance is observed at various locations of the washed sample's surface.

The washing stability of a wearable e-textiles could be improved either by a pretreatment such as with Bovine Serum Albumin (BSA)^[49] that can act as a molecular glue to bind graphene-based material, or via a posttreatment such as embedding with polydimethylsiloxane (PDMS),^[50,51] polyurethane (PU) sealing,^[52] a screen printed PU top layer,^[53] and transferred mold or hot melt encapsulation^[54] to seal the metal-based conductive track onto the textile surface. The failure rate with transfer mold is very high, whereas the hot melting creates a stiff surface which is also unsuitable for thermal stress. Here, a translucent, thin, and stretchable PU-based encapsulant was used to protect graphene-based wearable e-textiles. Such encapsulation material adheres with the textile material, as it anchors the conductive graphene flakes to the textile (Figure 2b). Moreover, it forms a fine encapsulation layer around individual G-coated textiles fibers, and allows air to pass through the gap between the fibers to enable breathable and comfortable e-textiles.

The washing stability performance of both coated and compressed graphene-based textiles after encapsulation was evaluated, where they show slight linear increment in resistance after each washing cycle (Figure 2a). The uncompressed G-coated and encapsulated graphene-based e-textiles show ≈ 10 times higher resistance after 10 washes, whereas G-coated, compressed and encapsulated graphene-based e-textiles provide only 3.5 times higher resistance after 10 washing cycles. This may be due to a flat surface and the better alignment of G flakes after compression, Figure 1i, whereas disoriented G flakes (Figure 2c) on an uncompressed surface are more prone to delamination due to the mechanical forces experienced during washing cycles, thus loses electrical conductivity.^[55] Figure 2d shows the removal of G flakes from the fiber surface without encapsulation after washing, whereas the encapsulated fiber surface shows more resistance to delamination as the graphene coating is protected by the thin PU layer (Figure 2e). Moreover, the digital images of the G-coated fabrics show the change of the color from black to grey after 10 washing cycles (Figure 2b, bottom). It is worth mentioning here that as encapsulation

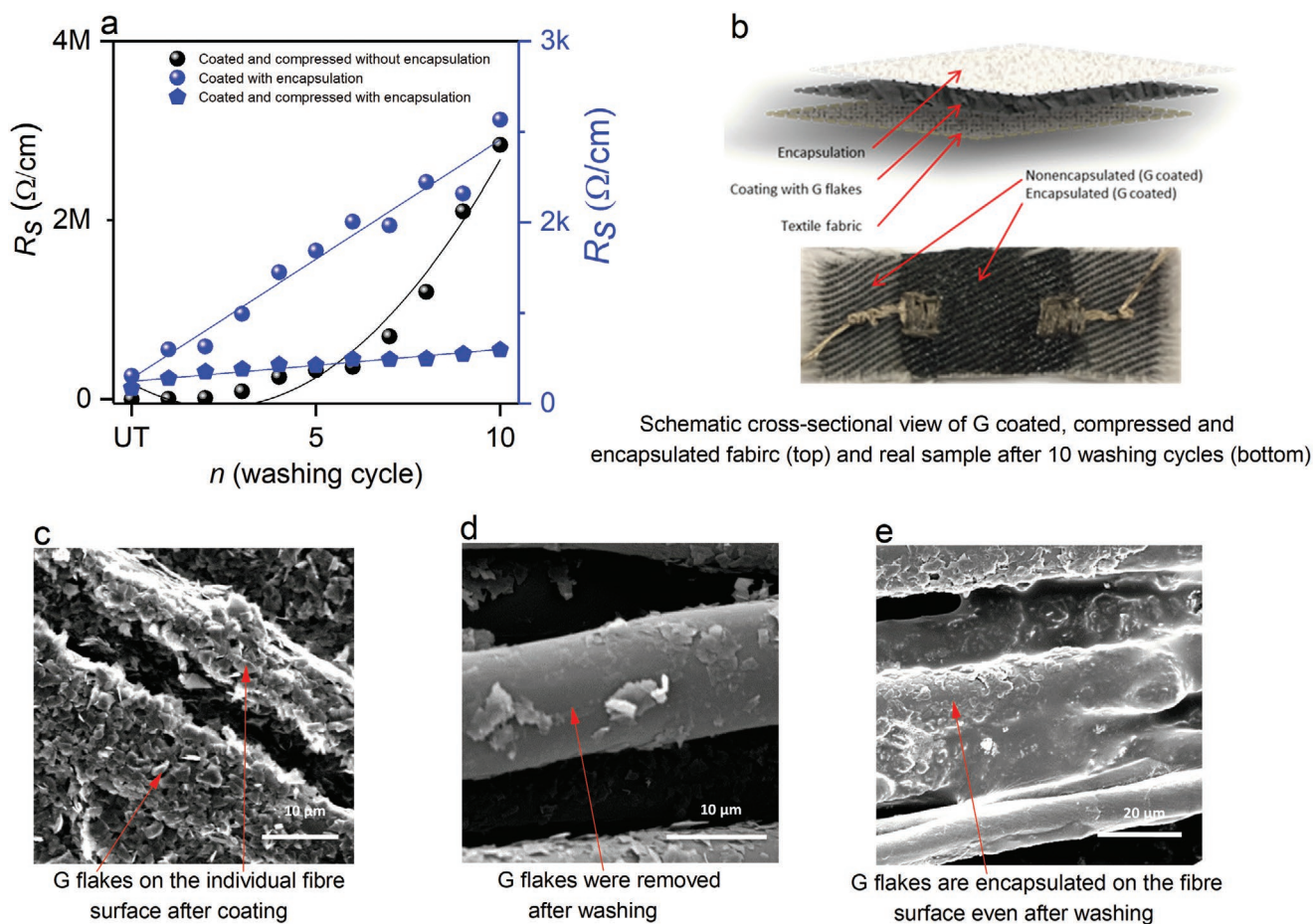


Figure 2. a) The change in resistance with the number of washing cycles of G-coated compressed (with encapsulation) poly-cotton fabric, G-coated only (with encapsulation) poly-cotton fabric, and G-coated compressed (without encapsulation) poly-cotton fabric. b) Graphical illustration of graphene and encapsulation layer on textile substrate (top), physical appearance of encapsulated, and nonencapsulated area of G-coated poly-cotton fabric after 10 washes (bottom). c) Scanning electron microscope (SEM) image of G-coated poly-cotton fiber (X5000). d) SEM image of G-coated poly-cotton fiber after washing (X5000). e) SEM image of as G-coated and encapsulated poly-cotton fiber after washing (X5000).

creates an insulating layer on a conductive surface, so a conductive pathway was established before encapsulation and washing by sewing sliver yarn into the graphene fabrics. The resistance per unit length (cm) of unwashed and washed samples was then measured via a multimeter to observe the effect of washing cycles on the conductivity.

2.3. Ultraflexible Graphene-Based Wearable E-Textiles

Here, the ultraflexibility of highly conductive and machine washable graphene e-textiles is demonstrated for wearable sensing applications. G-coated (5 passes), compressed and encapsulated poly-cotton fabrics were tested before and after washing (10 washing cycles) using a tensile tester. The change in their electrical resistances per 8 cm length during bending and compression both in forward and backward direction is measured. Here, the cord length is measured by the distance between the tensile tester grips during the experiment. The cord length changes (20–80 mm) as the fabrics are bent and compressed in both forward and backward directions. **Figure 3a–d** shows a repeatable response in the change of

resistance ($\Delta R/R_0$) in both forward and backward directions during bending and compression for before and after washed samples.^[21,56] Moreover, the variation of resistances is almost stable when both unwashed and washed samples were subject to 10 violent folding–releasing operations (**Figure 3e**). Similarly, the resistance changes barely upto 100 bending and releasing cycles for both before and after washed samples (**Figure 3f**). In addition, no visible changes in appearance or shape or creasing were observed due to such aggressive mechanical actions such as bending, compression, and folding cycles. This demonstrates the excellent flexibility and bendability of encapsulated and machine washable graphene-based wearable e-textiles.

2.4. Scalable, Ultraflexible, and High-Performance Supercapacitor

Here, one of the potential applications for the ultraflexible, highly conductive, and machine washable graphene-based e-textiles for ultraflexible supercapacitor is demonstrated. As seen from the SEM images of graphene-based textiles (**Figure 2c** and **Figure S3**, Supporting Information), the graphene flakes

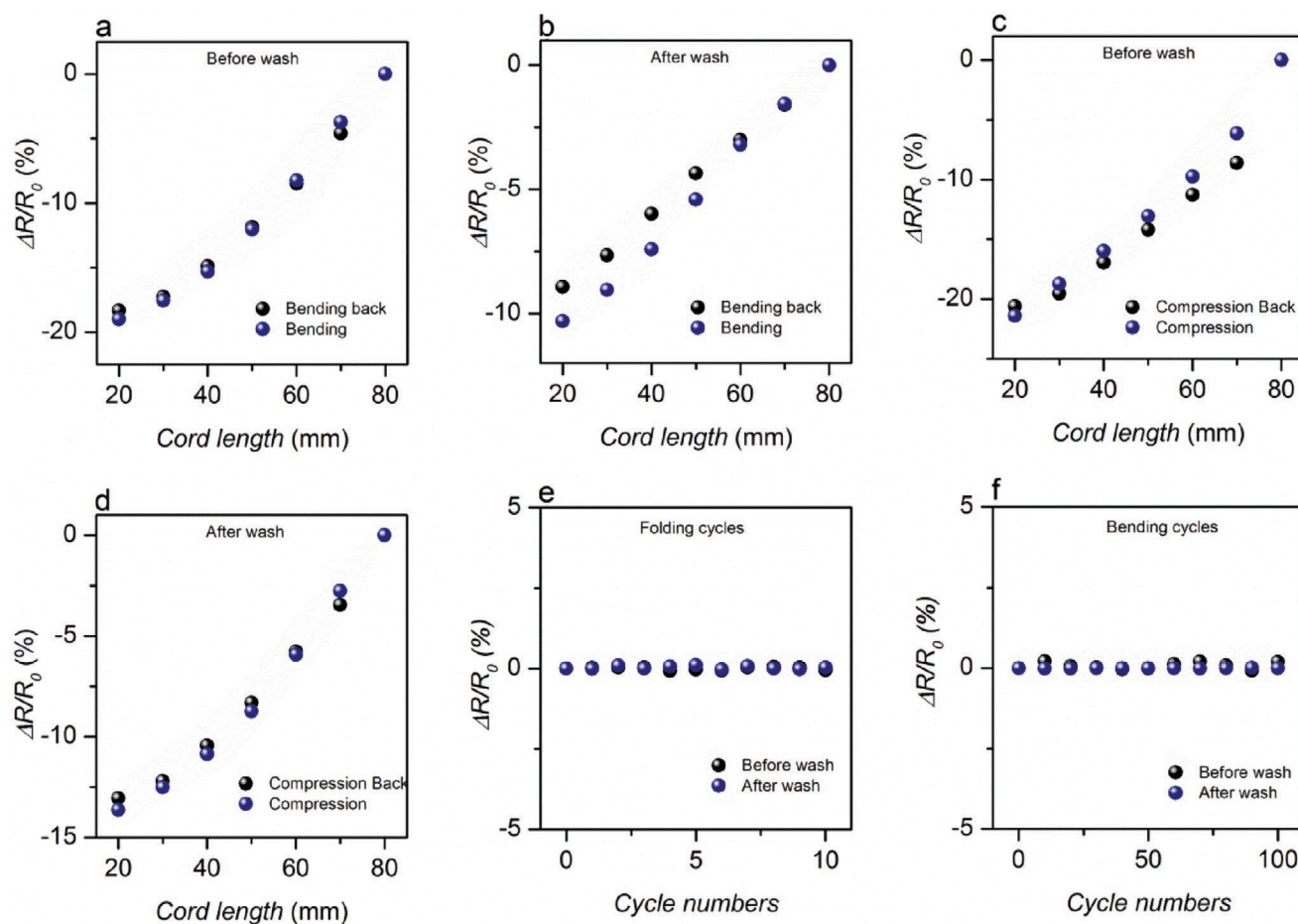


Figure 3. a) The variation in resistance of the bending sensor in forward (bending) and reverse (bending back) direction before wash. b) The variation in resistance of the bending sensor in forward (bending) and reverse (bending back) direction after wash. c) The variation in resistance of the compression sensor in forward (compression) and reverse (compression back) direction before wash. d) The variation in resistance of the compression sensor in forward (compression) and reverse (compression back) direction after wash. e) The variation in resistance under 10 folding–releasing cycles for before and after washed samples. f) The variation in resistance under cyclic bending for 100 times for before and after washed samples.

assemble themselves by forming a porous film on the textile with nano- and microchannels, due to the wide distribution of size and thickness. A structure like that would facilitate the interaction between the graphene coating and any electrolytes that can wet the surface, which is of particular interest for the energy storage application. Coupled with the higher conductivity and outstanding mechanical flexibility, the G-coated textiles may be a perfect candidate electrode for flexible energy storage devices. To prove this concept, a flexible supercapacitor device using two identical graphene-based e-textile electrodes and a hydrogel–polymer electrolyte based on poly(vinyl alcohol) (PVA) doped with H_2SO_4 was fabricated. The graphene-coated textile acts as a current collector, and the electrodes are connected directly to the potentiostat terminals. **Figure 4a** shows cyclic voltammograms (CV) reordered for the supercapacitor device at different scan rates. The CV curves are of rectangular shape within the potential window, indicating that the capacitance source is dominated by double layer phenomenon. It is well known that the surface of cotton textile is covered by various oxygen-containing groups. The absence of any redox peaks in the CV confirms the purity of the graphene flakes

and homogeneous covering for the cotton substrate. The CV curves maintain the rectangular shape and good mirror images with respect to zero-current line even at a scan rate as high as 1000 mV s^{-1} (Figure S5a, Supporting Information), demonstrating a fast charge transfer within the graphene layer due to its highly porous structure.

The galvanostatic charge–discharge analysis was used for practical evaluation of the capacitance of graphene textile electrodes. The curves obtained in Figure S5b, Supporting Information, show a nearly triangular shape with symmetrical charge and discharge branches, which confirm the ideal double layer capacitance, in accordance with the CV results. The areal capacitance calculated from the discharge curve at various current densities is shown in Figure 4c. The graphene-based (G-coated) textile electrodes can reach a maximum areal capacitance of $\approx 2.7 \text{ mF cm}^{-2}$, which is comparable with that recorded for the rGO electrodes ($\approx 2.4 \text{ mF cm}^{-2}$, Table S2, Supporting Information). Graphene oxide produced by the traditional Hummers methods consists mainly of the single layer flakes, which are supposed to provide a larger specific surface area and better near surface reactions than graphene platelets. However, rGO

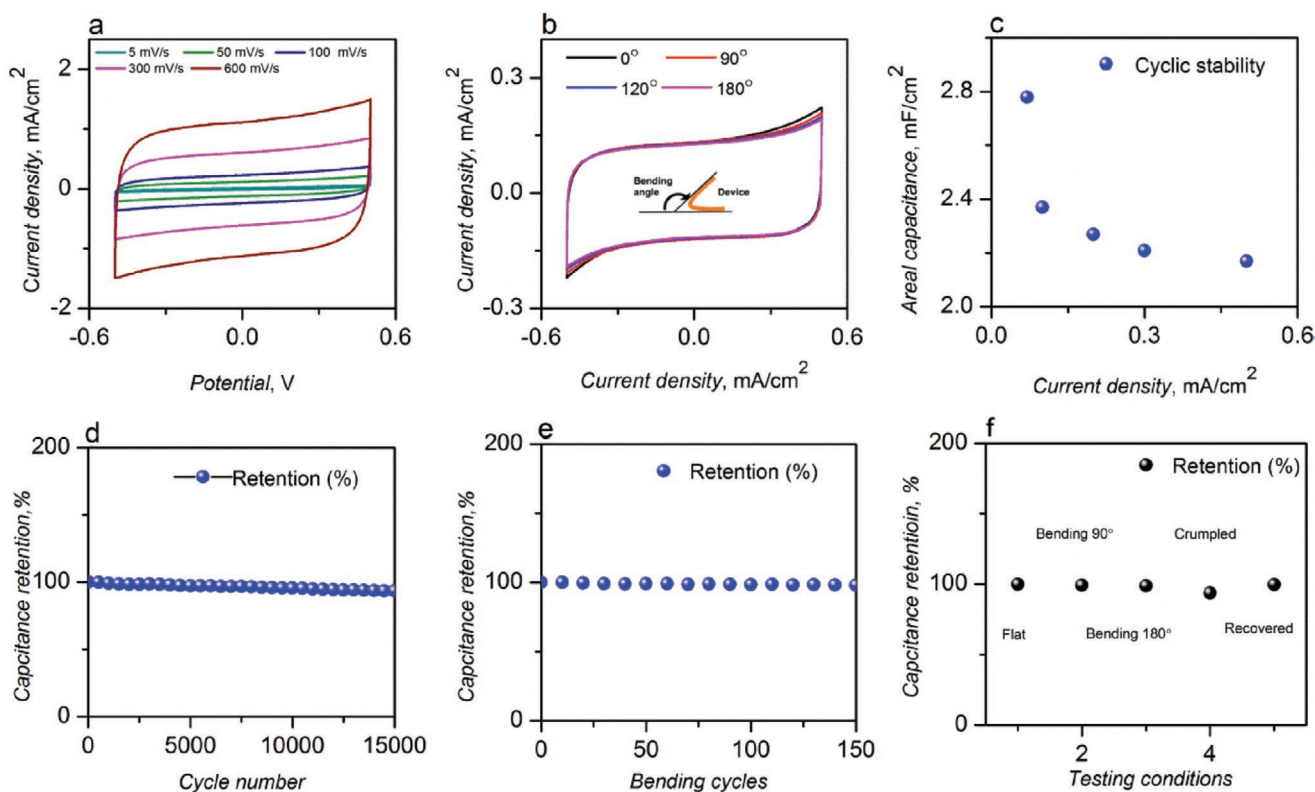


Figure 4. a) Cyclic voltammograms (CV) recorded for the supercapacitor device at different scan rates. b) CV curves for the ASC device at different bending angle. c) Effect of current density on the areal capacitance. d) Cyclic stability of the device. e) Stability of the device after 180° bending cycles. f) The capacitance retentions at various mechanical actions showing extremely high flexibility of the device.

flakes tend to aggregate and restack via van der Waal force, which reduces the surface of the electrode available for the electrochemical interaction. While graphene platelets also aggregate in a similar way, the smaller particles work as a spacer between the larger particles, leaving a large part of the electrode volume as porous connected channels. The arrangement of the graphene nanoplatelets in this highly porous architecture helps to overcome the limited specific surface area of rather thick flakes. Our SC device also shows excellent cyclability as it retains $\approx 98\%$ of its initial specific capacitance after 15 000 cycles (Figure 4d). This demonstrates excellent rate capability and a higher degree of reversibility at high charging–discharging rates.

The electrochemical stability of the graphene-coated textile supercapacitor was tested using a bending test. The CV curve of the flexible device was recorded at different bending angles and plotted in Figure 4e. The CV curves still maintain rectangular shape with no distortion at various bending angles, indicating the excellent flexibility of the supercapacitors. We have also measured the capacitance of a crumpled device (Figure 4f) and observed only 7% decrease in the total capacitance, showing that the device can sustain complex strain loading in various directions. The device maintains more than 98% of its initial capacitance after being subjected to 150 cycles of bending at 180° (Figure 5f). Moreover, we rolled the 20 cm² devices over a 10 mm diameter plastic bar and observed almost no decrease in the total capacitance of a flat device (Figure 4f). The excellent mechanical and electrochemical stability of the device is encouraging for flexible electronic applications.

For practical applications, large area supercapacitor that can store more energy is required by most engineers. The performance of the flexible energy storage devices always decreases with scaling up of the devices, and in term of the areal capacitance, it is always lower for larger areas. To test the viability of scaling up the supercapacitor, the areal capacitance is measured for devices with total area of 2, 5, 10, and 20 cm². Figure S5c, Supporting Information, shows the change in the total calculated capacitance as a function of the device surface area. The increase in the total capacitance is almost linear with small diversion from linearity for the larger area supercapacitors. Such results suggest low total resistance even for large area devices, which makes our graphene-coated textile promising candidate for large-scale flexible supercapacitor applications.

2.5. Activity Monitoring Strain Sensors via Graphene-Based E-Textiles

Wearable strain sensors, which can detect the mechanical deformations have attracted significant interests for motion monitoring of human body parts.^[57–61] In order to demonstrate other potential applications of graphene-based highly conductive textiles as skin-mounted strain sensors, graphene-coated, compressed and encapsulated textiles were attached on different parts of the body, for example index finger, wrist, and elbow joint (Figure 5d–f). The change of the resistances with the movement of various parts of the body before

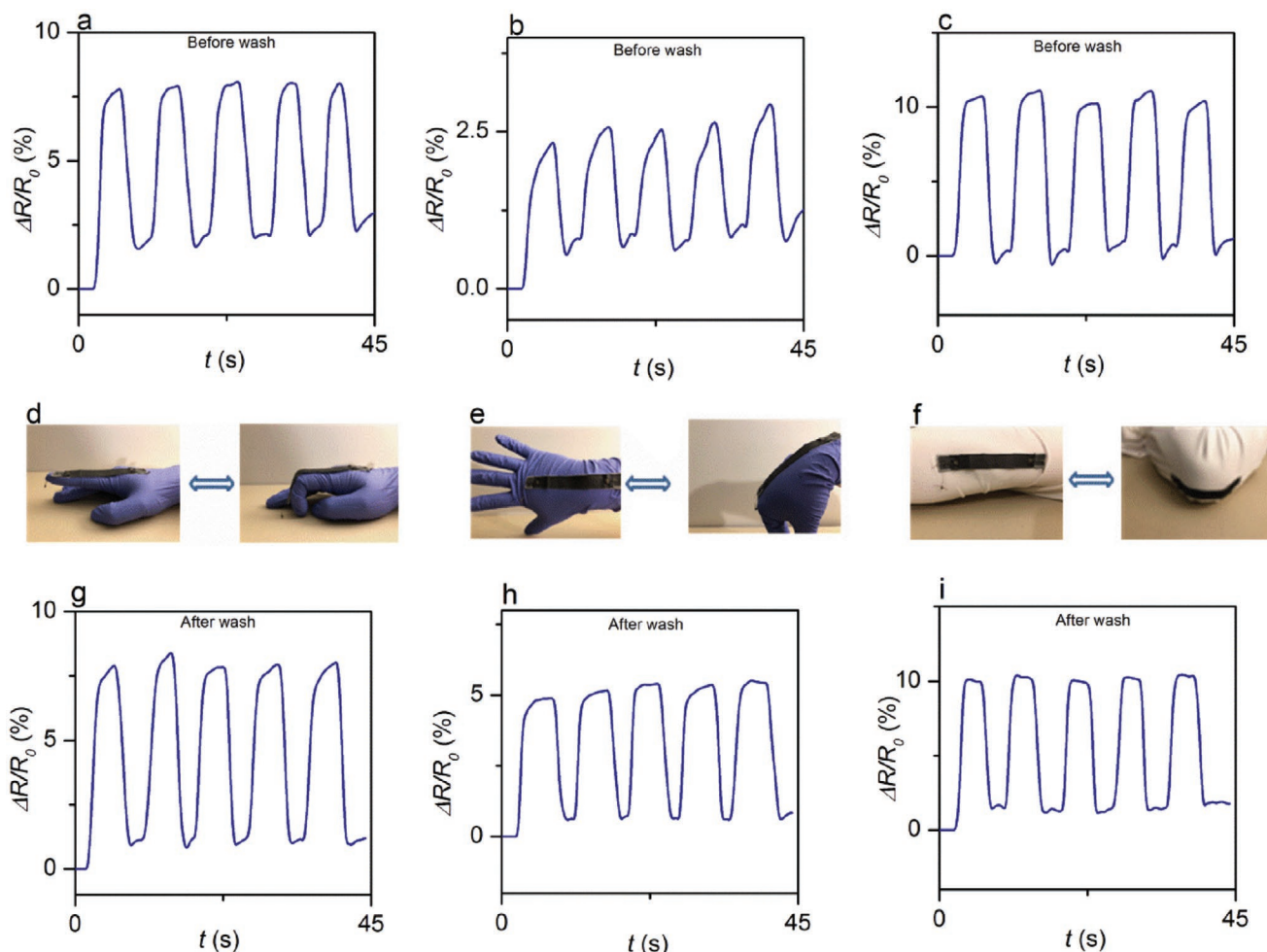


Figure 5. Application of highly conductive graphene-coated, compressed and encapsulated textiles as strain sensors to detect human motion (before wash): a) finger joint motion detection by compressed and encapsulated graphene textiles, b) wrist joint detection by compressed and encapsulated graphene textiles, and c) elbow joint motion detection by compressed and encapsulated graphene textiles. The photographs of the mounted strain sensor: d) on the finger, e) on the wrist joint, and f) on the elbow joint. Application of highly conductive graphene-coated, compressed and encapsulated textiles as strain sensors to detect human motion (after wash): g) finger joint motion detection by compressed and encapsulated graphene textiles, h) wrist joint detection by compressed and encapsulated graphene textiles and i) elbow joint motion detection by compressed and encapsulated graphene textiles.

(Figure 5a–c) and after wash samples (Figure 5g–i) are measured. Figure 5a–c shows repeatable responses of the change of resistance over time and excellent capability of capturing mechanical events such as upward–downward and bending–unbending movement of our graphene textiles-based strain sensors.

As the wash stability of such devices are extremely important for wearable e-textiles application, the compressed and encapsulated graphene-based textiles was washed using 10 home laundry wash cycles following a British standard (BS EN ISO 105 C06 A1S). The similar sensitivity measurements were performed on washed (10 times) and skin-mounted strain sensor. Like unwashed devices, Figure 5g,h shows similar repeatable response and excellent capability of compressed, encapsulated, and washed graphene-coated samples to capture mechanical events. As evident from SEM images (Figure 2e), a thin layer of encapsulation on graphene-coated textiles helps to hold graphene flakes on the fiber surface

without any breakages during washing cycles and other mechanical actions. It demonstrates excellent wash stability of graphene-based textiles for potential wearable electronics applications.

3. Conclusion

A simple and highly scalable way of producing ultraflexible, highly conductive, and machine washable graphene-based wearable e-textiles is reported. The graphene-based e-textiles thus produced exhibit the lowest sheet resistance ever reported on graphene-based textiles and the highest stability to repeated home laundry washes. The multifunctional uses of such graphene e-textiles are also demonstrated such as ultraflexible wearable sensor and flexible supercapacitor. The obtained result would enable development of next generation graphene-based wearable e-textiles for multifunctional applications.

4. Experimental Section

Materials: Natural flake graphite (average lateral size $\approx 50 \mu\text{m}$) was kindly supplied by Graphexel Limited, UK. Sodium deoxycholate (SDC) powder and microcircuit encapsulant PE773 are purchased from Sigma–Aldrich and Dupont, respectively. 65/35 poly-cotton 2/1 twill fabric was internally woven in the University of Manchester weaving laboratory, desized, scoured, and bleached to prepare ready-to-dye fabric.

Microfluidic Exfoliation of Graphene-Based Dispersions: A microfluidization technique was used to exfoliate highly conductive graphene-based dispersions.^[24,27] In brief, 100 g graphite powder was mixed with 1 L deionized (DI) water, and 10 g SDC was added to the dispersion and sonicated for 30 min. This dispersion was then passed through Z-type microfluidic channels of ≈ 200 and $\approx 87 \mu\text{m}$ diameter at high pressure (200 MPa) and 100 mL min^{-1} flow rate, which would apply high shear (10^8 s^{-1}) and exfoliate the graphite into a few layers of graphene (G). This process was repeated for 20 times, which was then used as conductive ink for coating textile fabrics.

Continuous Coating of Textiles with Graphene Ink: A simple laboratory scale pad–dry–cure method was used to coat textile fabric with conductive graphene materials and then batch dried with a Mathis Laboratory dryer (Mathis, Switzerland) at 100 °C for 5 min. The padding roller pressure and speed were adjusted to achieve 80–90 wt pick-up% of liquor on the weight of the fabric (o.w.f.). Each padding cycle included one padding and one drying pass. Samples were repeatedly pad-dried to optimize the number of padding (coating) cycles. The curing time and temperature were also optimized using a range of curing times (5–30 min) and temperatures (100 °C–200 °C).

Compression and Encapsulation of Graphene-Based E-Textiles: MSK-HRP roller compressor was used to compress the graphene-coated fabric. Graphene-based e-textiles was encapsulated with a fine layer of a microcircuit encapsulant PE773 using a simple hand screen printing technique. The samples were dried and cured at 150 °C for 1 min.

Characterization of Graphene-Based Dispersions and E-Textiles: The graphene dispersion was diluted to around 1 mg mL^{-1} solution and drop-casted on a Si–SiO₂ wafer (290 nm oxide on plain silicon) for measuring the flake thickness, flake size, and Raman analysis. Raman spectra and images were taken from 10 different locations on the sample and mean values were calculated. High definition optical microscope (Nikon DS–Ri2, Japan) was used to measure the flake size from images.

The surface topography of the control poly-cotton, graphene-coated poly-cotton, graphene-coated washed poly-cotton, graphene-coated and encapsulated washed poly-cotton, and graphene-coated and compressed poly-cotton was analyzed using a Zeiss ultra scanning electron microscope (SEM). Dimension Icon (Bruker) atomic force microscopy (AFM) was used to measure the flake thickness of G flakes. A Renishaw Raman System equipped with a 633 nm laser was used for Raman spectroscopy analysis. The surface functionality of G flake and starting graphite was characterized using a Kratos axis X-ray photoelectron spectroscopy (XPS) system. The wash stability of graphene material coated fabric was carried out according to BS EN ISO 105 C06 A1S as previously reported.^[21]

Kawabata test was conducted to evaluate the shear rigidity and shear hysteresis of G-coated fabric and characterize the fabric handle qualities (e.g., softness or stiffness and smoothness perceived by human touch).^[43] The sheet resistance was measured by Jandel four-point probe system (Jandel Engineering Ltd., Leighton, UK). For wash-ability test, a conductive patch was created with electrically conductive silver thread to measure the resistance of encapsulated graphene-coated fabric using a standard multimeter.

By following previously reported methods,^[12,21] various cord lengths were used during bending and compression to measure the change of resistance of both washed and unwashed graphene-coated, compressed and encapsulated fabric (8 cm length). A Zwick–Roell tensile tester (Zwick Roell Group, Germany) was used to control the cord length during bending, compression, and folding cycles tests in both the forward and reverse directions. The change of the resistance of G-coated fabrics during various mechanical actions such as bending, compression, and folding, and also skin-mounted sensors on index

fingers, wrist, and elbows was captured using a National Instrument 9219 data acquisition card (NI, American). Informed consent was obtained from the researcher who performed the experiment.

Supercapacitor Device Fabrication and Electrochemical Characterization: G-coated poly-cotton fabric was used as current collector and glue a copper sheet to the end of each current collector. Following previously reported work,^[62] two pieces of G-coated fabric were coated with a hydrogel–polymer electrolyte, PVA doped with H₂SO₄, and then left overnight at room temperature to dry and remove excess water. In order to form an integrated device, two electrodes were pressed together under ≈ 1 MPa pressure for 10 min. The electrochemical performances such as CV and galvanostatic charge–discharge was investigated on an Ivium Potentiostat Electrochemical Interface.

Supporting Information

Supporting Information is available from the Wiley Online Library or from the author.

Acknowledgements

The authors acknowledge the Government of Bangladesh for funding this work by providing Ph.D. scholarship to S.A. The authors also acknowledge the funding from EU Graphene Flagship Program, European Research Council Synergy Grant Hetero2D, the Royal Society, and Engineering and Physical Sciences Research Council, UK (EPSRC Grant No. EP/N010345/1, 2015).

Conflict of Interest

The authors declare no conflict of interest.

Author Contributions

S.A. conceived, designed and conducted most of the experiments under supervision of N.K. and K.S.N. S.T. carried out flexibility and skin mounted sensors measurements under supervision of N.K. A.A. prepared and carried out flexible supercapacitor measurements and characterisation. S.A. and N.K. wrote the manuscript with inputs from K.S.N and A.A.

Keywords

e-textiles, graphene, sensors, supercapacitors, wearables

Received: January 12, 2020

Revised: February 26, 2020

Published online: April 8, 2020

- [1] L. Hu, M. Pasta, F. La Mantia, L. Cui, S. Jeong, H. D. Deshazer, J. W. Choi, S. M. Han, Y. Cui, *Nano Lett.* **2010**, *10*, 708.
- [2] S. Pan, H. Lin, J. Deng, P. Chen, X. Chen, Z. Yang, H. Peng, *Adv. Energy Mater.* **2015**, *5*, 1401438.
- [3] R. Paradiso, G. Loriga, N. Taccini, *IEEE Trans. Inf. Technol. Biomed.* **2005**, *9*, 337.
- [4] J. Meyer, P. Lukowicz, G. Troster, presented at 10th IEEE Int. Symon Wearable Computers, Montreux October **2006**.
- [5] S. Park, S. Jayaraman, *MRS Bull.* **2003**, *28*, 585.
- [6] B. S. Shim, W. Chen, C. Doty, C. Xu, N. A. Kotov, *Nano Lett.* **2008**, *8*, 4151.

- [7] Z. Zhao, C. Yan, Z. Liu, X. Fu, L. M. Peng, Y. Hu, Z. Zheng, *Adv. Mater.* **2016**, *28*, 10267.
- [8] T. Lanz, A. Sandström, S. Tang, P. Chabreck, U. Sonderegger, L. Edman, *Flexible Printed Electron.* **2016**, *1*, 025004.
- [9] F. Xu, Y. Zhu, *Adv. Mater.* **2012**, *24*, 5117.
- [10] L. Shu, T. Hua, Y. Wang, Q. Li, D. D. Feng, X. Tao, *IEEE Trans. Inf. Technol. Biomed.* **2010**, *14*, 767.
- [11] A. Lanatà, E. P. Scilingo, in *Autonomous Sensor Networks: Collective Sensing Strategies for Analytical Purposes* (Ed.: D. Filippini), Springer, Berlin, Heidelberg **2013**, p. 127.
- [12] S. Afroj, N. Karim, Z. Wang, S. Tan, P. He, M. Holwill, D. Ghazaryan, A. Fernando, K. S. Novoselov, *ACS Nano* **2019**, *13*, 3847.
- [13] W. Zeng, L. Shu, Q. Li, S. Chen, F. Wang, X. M. Tao, *Adv. Mater.* **2014**, *26*, 5310.
- [14] N. Karim, S. Afroj, S. Tan, K. S. Novoselov, S. G. Yeates, *Sci. Rep.* **2019**, *9*, 8035.
- [15] M. Irimia-Vladu, E. D. Głowacki, G. Voss, S. Bauer, N. S. Sariciftci, *Mater. Today* **2012**, *15*, 340.
- [16] K. S. Novoselov, A. K. Geim, S. V. Morozov, D. Jiang, Y. Zhang, S. V. Dubonos, I. V. Grigorieva, A. A. Firsov, *Science* **2004**, *306*, 666.
- [17] A. K. Geim, *Science* **2009**, *324*, 1530.
- [18] K. S. Novoselov, V. I. Fal'ko, L. Colombo, P. R. Gellert, M. G. Schwab, K. Kim, *Nature* **2012**, *490*, 192.
- [19] F. Sarker, P. Potluri, S. Afroj, V. Koncherry, K. S. Novoselov, N. Karim, *ACS Appl. Mater. Interfaces* **2019**, *11*, 21166.
- [20] F. Sarker, N. Karim, S. Afroj, V. Koncherry, K. S. Novoselov, P. Potluri, *ACS Appl. Mater. Interfaces* **2018**, *10*, 34502.
- [21] N. Karim, S. Afroj, S. Tan, P. He, A. Fernando, C. Carr, K. S. Novoselov, *ACS Nano* **2017**, *11*, 12266.
- [22] N. Karim, S. Afroj, A. Malandraki, S. Butterworth, C. Beach, M. Rigout, K. S. Novoselov, A. J. Casson, S. G. Yeates, *J. Mater. Chem. C* **2017**, *5*, 11640.
- [23] S. Pei, H. M. Cheng, *Carbon* **2012**, *50*, 3210.
- [24] N. Karim, M. Zhang, S. Afroj, V. Koncherry, P. Potluri, K. S. Novoselov, *RSC Adv.* **2018**, *8*, 16815.
- [25] T. Panagiotou, J. M. Bernard, S. V. Mesite, presented at Nano Science and Technology Institute (NSTI) Conf. Expo Proceed., Boston June **2008**.
- [26] S. M. Jafari, Y. He, B. Bhandari, *J. Food Eng.* **2007**, *82*, 478.
- [27] P. G. Karagiannidis, S. A. Hodge, L. Lombardi, F. Tomarchio, N. Decorde, S. Milana, I. Goykhman, Y. Su, S. V. Mesite, D. N. Johnstone, R. K. Leary, P. A. Midgley, N. M. Pugno, F. Torrissi, A. C. Ferrari, *ACS Nano* **2017**, *11*, 2742.
- [28] C. Kallmayer, R. Pisarek, S. Cichos, A. Neudeck, S. Gimpel, presented at Electronic Components and Technology Conference, New Orleans, LA May **2003**.
- [29] L. Xu, G. Yang, H. Jing, J. Wei, Y. Han, *Nanotechnology* **2014**, *25*, 055201.
- [30] R. R. Sondergaard, N. Espinosa, M. Jørgensen, F. C. Krebs, *Energy Environ. Sci.* **2014**, *7*, 1006.
- [31] L. Malard, M. Pimenta, G. Dresselhaus, M. Dresselhaus, *Phys. Rep.* **2009**, *473*, 51.
- [32] A. M. Abdelkader, I. A. Kinloch, *ACS Sustainable Chem. Eng.* **2016**, *4*, 4465.
- [33] A. M. Abdelkader, H. V. Patten, Z. Li, Y. Chen, I. A. Kinloch, *Nanoscale* **2015**, *7*, 11386.
- [34] M. J. Fernández-Merino, L. Guardia, J. I. Paredes, S. Villar-Rodil, P. Solís-Fernández, A. Martínez-Alonso, J. M. D. Tascón, *J. Phys. Chem. C* **2010**, *114*, 6426.
- [35] I. K. Moon, J. Lee, R. S. Ruoff, H. Lee, *Nat. Commun.* **2010**, *1*, 73.
- [36] S. Stankovich, D. A. Dikin, R. D. Piner, K. A. Kohlhaas, A. Kleinhammes, Y. Jia, Y. Wu, S. T. Nguyen, R. S. Ruoff, *Carbon* **2007**, *45*, 1558.
- [37] D. A. Brownson, S. A. Varey, F. Hussain, S. J. Haigh, C. E. Banks, *Nanoscale* **2014**, *6*, 1607.
- [38] J. Benson, Q. Xu, P. Wang, Y. Shen, L. Sun, T. Wang, M. Li, P. Papakonstantinou, *ACS Appl. Mater. Interfaces* **2014**, *6*, 19726.
- [39] Y. Gao, W. Shi, W. Wang, Y. Leng, Y. Zhao, *Ind. Eng. Chem. Res.* **2014**, *53*, 16777.
- [40] O. C. Compton, S. T. Nguyen, *Small* **2010**, *6*, 711.
- [41] M. Dzięcioł, J. Trzeczcyński, *J. Appl. Polym. Sci.* **1998**, *69*, 2377.
- [42] M. Lewin, *Polym. Degrad. Stab.* **2005**, *88*, 13.
- [43] S. Kawabata, M. Niwa, *J. Text. Inst.* **1989**, *80*, 19.
- [44] Y. J. Yun, W. G. Hong, W. J. Kim, Y. Jun, B. H. Kim, *Adv. Mater.* **2013**, *25*, 5701.
- [45] X. Huang, T. Leng, X. Zhang, J. C. Chen, K. H. Chang, A. K. Geim, K. S. Novoselov, Z. Hu, *Appl. Phys. Lett.* **2015**, *106*, 203105.
- [46] H. Malekpour, K. H. Chang, J. C. Chen, C. Y. Lu, D. L. Nika, K. S. Novoselov, A. A. Balandin, *Nano Lett.* **2014**, *14*, 5155.
- [47] X. Huang, T. Leng, M. Zhu, X. Zhang, J. Chen, K. Chang, M. Aqeeli, A. K. Geim, K. S. Novoselov, Z. Hu, *Sci. Rep.* **2016**, *5*, 18298.
- [48] K. Arapov, K. Jaakkola, V. Ermolov, G. Bex, E. Rubingh, S. Haque, H. Sandberg, R. Abbel, G. With, H. Friedrich, *Phys. Status Solidi RRL* **2016**, *10*, 812.
- [49] Y. J. Yun, W. G. Hong, D. Y. Kim, H. J. Kim, Y. Jun, H.-K. Lee, *Sens. Actuators, B* **2017**, *248*, 829.
- [50] T. Vervust, G. Buyle, F. Bossuyt, J. Vanfleteren, *J. Text. Inst.* **2012**, *103*, 1127.
- [51] Y. Liu, K. N. Zhang, Y. Zhang, L. Q. Tao, Y. X. Li, D.-Y. Wang, Y. Yang, T. L. Ren, *Appl. Phys. Lett.* **2017**, *110*, 261903.
- [52] J. Cho, J. Moon, K. Jeong, G. Cho, *Fibers Polym.* **2007**, *8*, 330.
- [53] W. G. Whittow, A. Chauraya, J. C. Vardaxoglou, Y. Li, R. Torah, K. Yang, S. Beeby, J. Tudor, *IEEE Antennas Wireless Propag. Lett.* **2014**, *13*, 71.
- [54] T. Linz, R. Vieroth, C. Dils, M. Koch, T. Braun, K. F. Becker, C. Kallmayer, S. M. Hong, *Adv. Sci. Technol.* **2008**, *60*, 85.
- [55] A. Chatterjee, M. Nivas Kumar, S. Maity, *J. Text. Inst.* **2017**, *108*, 1910.
- [56] Y. Cheng, R. Wang, J. Sun, L. Gao, *Adv. Mater.* **2015**, *27*, 7365.
- [57] Y. Qiao, Y. Wang, H. Tian, M. Li, J. Jian, Y. Wei, Y. Tian, D. Y. Wang, Y. Pang, X. Geng, X. Wang, Y. Zhao, H. Wang, N. Deng, M. Jian, Y. Zhang, R. Liang, Y. Yang, T. L. Ren, *ACS Nano* **2018**, *12*, 8839.
- [58] J. Zhang, L. Wan, Y. Gao, X. Fang, T. Lu, L. Pan, F. Xuan, *Adv. Electron. Mater.* **2019**, *5*, 1900285.
- [59] Y. Z. Zhang, K. H. Lee, D. H. Anjum, R. Sougrat, Q. Jiang, H. Kim, H. N. Alshareef, *Sci. Adv.* **2018**, *4*, eaat0098.
- [60] Q. Li, K. Wang, Y. Gao, J. P. Tan, R. Y. Wu, F. Z. Xuan, *Appl. Phys. Lett.* **2018**, *112*, 263501.
- [61] Y. Gao, Q. Li, R. Wu, J. Sha, Y. Lu, F. Xuan, *Adv. Funct. Mater.* **2019**, *29*, 1806786.
- [62] A. M. Abdelkader, N. Karim, C. Vallés, S. Afroj, K. S. Novoselov, S. G. Yeates, *2D Mater.* **2017**, *4*, 035016.